Interactions from lipid membrane deformations

Azadbakht, A.

Chapter 2

Wrapping pathways of anisotropic dumbbell particles by giant unilamellar vesicles

Abstract: Endocytosis is a key cellular process involved in the uptake of nutrients, pathogens or the therapy of diseases. Most studies have focused on spherical objects, whereas biologically relevant shapes can be highly anisotropic. In this chapter, we use an experimental model system based on Giant Unilamellar Vesicles (GUVs) and dumbbell-shaped colloidal particles to mimic and investigate the first stage of the passive endocytic process: engulfment of an anisotropic object by the membrane. Our model has specific ligand-receptor interactions realized by mobile receptors on the vesicles and immobile ligands on the particles. Through a series of experiments, theory and molecular dynamics simulations, we quantify the wrapping process of anisotropic dumbbells by GUVs and identify distinct stages of the wrapping pathway. We find that the strong curvature variation in the neck of the dumbbell as well as membrane tension are crucial in determining both the speed of wrapping and the final states.

2.1 Introduction

The engulfment of objects through the cell membrane is critical for endocytic processes such as phagocytosis [112–114] and receptor-mediated endocytosis. The latter is often exploited by viruses for cell entry and proliferation [115] and key to nanomedical applications such as drug delivery and imaging [116]. To single out receptor-mediated effects from active mechanisms involved in the engulfment [52], simplified passive model systems can be employed, which recently led to a conclusive understanding of the wrapping of spherical objects [57,58]. However, biological objects such as bacteria and viruses [115,117,118] as well as nanoparticles relevant for applications in nanomedicine but also nanotoxicology [119] often posses non-spherical shapes. Moreover, *in vitro* experiments with nanoparticles and simulations have shown that the size and shape influence their likelihood to be taken up by endocytosis [48, 52, 120–124].

The wrapping pathways of spheres at sufficiently low membrane tensions have been shown to be a continuous transition from attached to fully wrapped, occurring either spontaneously or after activation [55, 57, 58]. In contrast, anisotropic particles such as ellipsoids and rods, are expected to reorient during the wrapping process or become trapped in metastable states due to their varying curvature. [48, 64–66, 125–129] The aspect ratio of these particles as well as the degree of rounding of their tip were the key parameters affecting the wrapping orientation with respect to the membrane and their metastable and stable states [48,129]. Despite the extensive work in theory and simulations and exciting observations on shape-dependence in phagocytosis [130], no experimental work has investigated the passive wrapping process of anisotropic particles by lipid membranes and tested these predictions yet.

In this chapter, we employ an experimental model system based on Giant Unilamellar Vesicles (GUVs) and colloidal dumbbell particles to investigate the wrapping of micrometre-sized anisotropic objects by lipid membranes. Our model system is designed to have mobile ligands on the vesicles and immobile receptors on the particles mimicking receptor-mediated endocytotic systems [55, 56, 89]. We quantify the wrapping pathways of anisotropic dumbbells by lipid membranes

and test if their initial orientation affects the final states. Molecular dynamics simulations of the same system corroborate our experimental data, allowing us to inspect the dynamics of the process that was inaccessible to experiment. We find that the strong curvature variation in the neck of the dumbbell as well as membrane tension and not their initial orientation are crucial in both determining the speed of wrapping and the final states.

2.2 Materials and Methods

2.2.1 Materials

Chloroform ($CHCl_3$) 99.0-99.4%, D-glucose, EDC N-(3-Dimethylaminopropyl)-N'-ethylcarbodiimide hydrochloride (98%), Sulfo-NHS (N-Hydroxysulfosuccinimide sodium salt) were purchased from Sigma-Aldrich. DOPC (Δ 9-cis 1,2-dioleoyl-sn-glycero-3-phosphocholine), DOPE-rhodamine (1,2-dioleoyl-sn-glycero-3-phosphoethanolamine-N-(lissaminerhodamine B sulfonyl)), DOPE-PEG2000-biotin (1,2-dioleoyl-sn-glycero-3-phosphoethanolamine-N-[biotinyl(polyethylene glycol)-2000]) were purchased from Avanti Polar Lipids. Potassium chloride (KCl) 99+%, and Sodium azide (NaN_3) 99%, extra pure were provided from Acros Organics. Biotin-4-fluorescein ($C_{33}H_{32}N_4O_8S$) from Molecular Probes. mPEG5000-NH_2 Methoxypolyethylene glycol amine M.W. 5000 from Alfa Aesar. NeutrAvidin was bought from Thermo Fisher Scientific. Phosphate buffered saline (PBS) tablets from Merck Millipore. Ethanol (C_2H_5OH) from Honeywell, and water (H_2O) was filtered with a MilliQ MilliPore apparatus (resistivity 18.2 M$\Omega\cdot$ cm). All chemicals were used as received.

2.2.2 Membrane preparation

Electroformation was used to prepare GUVs with a diameter between 10 and 100 µm [131]. A lipid mixture containing 97.5 wt% DOPC, 2 wt% DOPE-PEG2000-biotin and 0.5 wt% DOPE-rhodamine was dissolved in chloroform at 1.45 g l^{-1}. Two 6 cm^2 ITO-coated glass slides (15-25 Ω m^{-1}) were spin coated with 10 µL lipid mixture each, using a SCS 6800 spin coater at 2000 rpm. The coated slides were dried in a vacuum chamber for 2 hours, after which they were placed in 1.8 ml of 100 mM glucose solution and connected to a function generator. An alternating current of 1.1 V(rms) at 10 Hz was applied for 3 hours. The GUVs were stored in a 2 ml Eppendorf tube at room temperature for a maximum of 4 days.

2.2.3 Particle Functionalization

Carboxylic acid functionalized polystyrene spheres with a diameter of 0.98 ± 0.03 µm were prepared using a surfactant-free dispersion polymerization protocol [132]. These spheres were coated with NeutrAvidin and mPEG5000-NH_2, based on a modified version of the protocol described in [59]. The modification enabled the particles to cluster and form dumbbells during the coating process. All reactions were performed at 4 °C. First, particles with concentration of 2%w/w were activated using 8 mM EDC and 2.5 mM Sulfo-NHS. After 30 minutes of vortexing,

1 µmol NeutrAvidin dissolved in 50 µL water was added to 750 µL of activated particles. After 2 hours of vigorous mixing with a vortex mixer, 200 µL water containing 4.0 mg dissolved mPEG5000-NH_2 was added and the entire solution was mixed using an orbital rotator at 30 RPM for 40 hours while still at 4 °C. Last, the coated particles were washed three times with water and 3 mM sodium azide was added to prevent bacterial growth.

The particles were coated with polyethylene glycol (PEG) to prevent them from clustering after synthesis. The PEG functionality of the particles was tested by placing the particles in a 1 M KCl solution for one hour. After one hour, no significant clustering of the particles was observed, concluding that the particles were successfully coated with PEG.

2.2.4 Imaging and optical tweezers setup

Imaging was performed on polyacrylamide-coated coverslips, which were prepared following a protocol based on [133]. The coverslips were washed thoroughly with water and PBS before use. Besides, GUVs were washed with PBS to remove undesired lipid structures. Samples were prepared by placing 400 µL of this mixture on a polyacrylamide-coated coverslip and kept open to evaporation to gradually increase osmolarity. A Nikon Eclipse Ti microscope with an A1R confocal scanning head and a 60× (NA = 1.2) water immersion objective were used to acquire all images. The sample was placed on a MCL Nano-Drive piezo to acquire high speed z-stack images. The attachment of a dumbbell to a GUV was established by bringing the particle within close proximity of the GUV using an optical tweezers setup. The optical trap is a home-built setup consisting of a highly focused 1064nm laser beam of Nd:YAG Opus purchased from LaserQUANTUM. The laser beam enters through the rear aperture of the microscope and is reflected by a dichroic mirror onto the rear pupil of the objective. While control of the particle position is very high, the orientational control is only approximate. Dumbbell colloids orient themselves in the trap such that their long axis lies perpendicular to the imaging plane. Approaching a GUV from the top, the particle typically adheres with only one lobe, whereas approaching it at the equator the particle is more likely to adhere with either both lobes or with a higher value of θ.

2.2.5 Analysis

All images were analysed with python. A tracking toolkit called Trackpy [134] and an extension based on this toolkit called Clustertracking [135] were used to determine the two dimensional coordinates of both lobes of the dumbbell particles. The two dimensional GUV contour was determined using a package called circletracking [136].

During the data acquisition, z-stack image sequences were captured for all examined GUVs. A z-stack image sequence consisted of multiple images recorded at different focal heights. By ascending the z-coordinate in small steps (typically 300 nm) from the bottom to the top of a GUV, the complete vesicle was imaged. The radius of the GUV was then determined from the equator image of the z-stack. All radii were determined by averaging over multiple equator images from different

z-stacks.

2.3 Results and Discussion

We investigate the wrapping process of anisotropic objects by a lipid membrane using a model system consisting of GUVs and colloidal particles, (see Figure 2.1a). We chose the simplest object that features anisotropy: a dumbbell shaped colloidal particle that consists of two equal sized spheres. The colloid dumbbells were obtained from aggregating polystyrene spheres with diameter d_s=0.98± 0.03 μm [59] by briefly lowering the pH to 5.3 and then quenching the process by increasing the pH to 8.6 [137]. This process yielded 5-10% dimers with a long axis of 1.96 ± 0.06 μm and a short axis of 0.98 ± 0.03 μm. The spherical particles that make up the dumbbells have previously been used in similar experiments [55], where it was found that increasing the adhesion energy increases the percentage of wrapped particles and that increasing the membrane tension precluded wrapping. In the current system we functionalized the particles with the highest concentration of ligands explored in Ref. [55] to enhance the probability of wrapping. GUVs were prepared by electroswelling from 97.5% w/w 1,2-dioleoyl-sn-glycero-3-phosphocholine (DOPC).

To realize strong ligand-receptor mediated binding we doped the GUVs with 2% w/w 1,2-dioleoyl-sn-glycero-3-phosphoethanolamine-N-[biotin-2000] (DOPE-PEG2000-Biotin) and the dumbbells with $2.2\times10^3/\mu m^2$ NeutrAvidin following [59], see Figure 2.1b and c and see particle functionalization in Methods 2.2.3 and quantification of binding affinity in Appendix2.5.1. We suppress electrostatic interactions by working in 50 mM Phosphate Buffered Saline, and achieve colloidal stability by coating the dumbbells with polyethyleneglycol (PEG5000). Imaging of the position and orientation of the dumbbells and membranes in three dimensions was made possible by dying the colloids with BODIPY, represented by a green color throughout the manuscript, as well as including 0.5% w/w 1,2-dioleoyl-sn-glycero-3-phosphoethanolamine-N-(lissamine rhodamine B sulfonyl) (DOPE-Rhodamine) into the GUVs, represented by a magenta color. See Figure 2.1c. Confocal stacks and image sequences were acquired with an inverted Nikon Ti-E microscope, equipped with a 60x (NA 1.2) objective and A1-R scan head. 2D image sequences were taken at 59 fps, which enables tracking of the dumbbells in real time. Experimental details are described in Appendix 2.5.2.

To initiate the wrapping process, we used optical tweezers to bring dumbbell particles in contact with the GUV. They subsequently diffused on the GUV surface before suddenly and quickly becoming wrapped, a process that took between a few seconds and a few minutes depending on membrane tension, see Figure 2.1e. To capture the wrapping process with high speed, we adjusted the focal height during acquisition of the image sequence. After wrapping, the dumbbell continued to diffuse on the inside of the vesicle.

We quantify the wrapping process of a dumbbell by measuring the angle θ between the major axis of the dumbbell and surface normal of the GUV and distance d of the dumbbell with respect to the undistorted surface of the GUV, see Figure 2.1d. We inferred the 3D position of the dumbbell from the position of its lobes with respect to the GUV. To improve the accuracy of tracking, particles

were tracked only when their center of mass was between -0.8R<z<0.8R, and when both lobes were in focus. Details are described in Appendix 2.5.2.

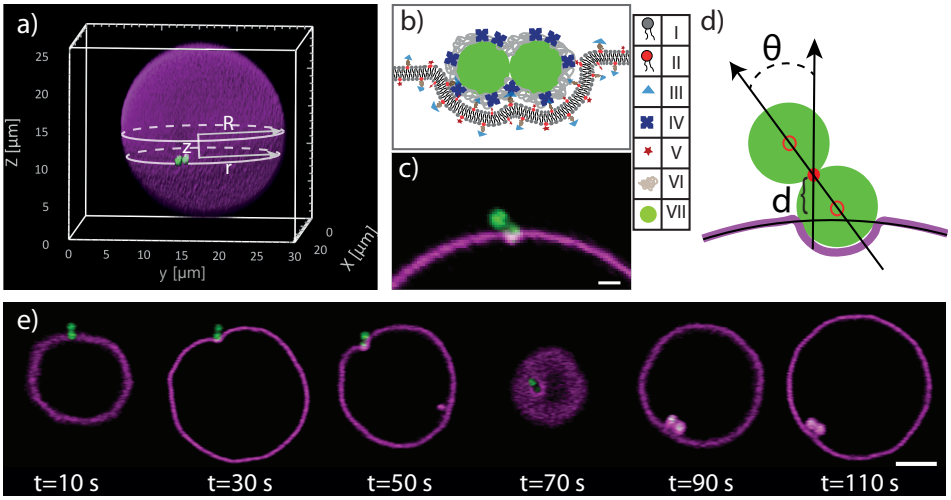

Figure 2.1: Experimental setup to quantitatively measure the wrapping process of a dumbbell colloid by a GUV a) 3D confocal reconstruction of a GUV in magenta and a dumbbell particle in green with an indication of the relative height z from the equator of the GUV, radius of GUV R, and cross section radius of the vesicle at the location of the dumbbell, r. b) Detailed schematic of ligand-receptor based binding scheme between the dumbbell and GUV. I-DOPC lipid II-DOPE lipid III-Biotin IV-NeutrAvidin V-Rhodamine, VI-Polyethylene glycol (PEG) VII-Polystyrene particle. (Not to scale); c) Representative confocal images reconstructed from two channels, (1) dumbbell excited by 488 nm laser light and emission; collected between 500 and 550 nm (depicted in green) and (2) GUV excited by 561 nm laser light and emission collected in 580−630 nm (depicted in magenta) (scale bar 1μm). d) Schematic representation of the parameters d and θ used for the quantitative description of the wrapping process. e) Time series of snapshots of confocal images of a dumbbell being wrapped by a vesicle (scale bar 4μm).

We show confocal microscopy snapshots of a typical wrapping pathway in Figure 2.1 e, and quantitative data of θ and d for exemplary pathways in Figure 2.2a and b. Surprisingly, we find that the dumbbells end up in one of two states, independent of their initial orientations: (1) both lobes are either being fully wrapped (Figure 2.2a, III), or (2) a single lobe is being wrapped, such that the dumbbell is engulfed up to its waist by the membrane (Figure 2.2b, VI). The green-blue points in Figure 2.2a and b represent dumbbells attached almost parallel to the membrane at the beginning of the process (Figure 2.2 I, IV), whereas the yellow-red points represent dumbbells attached roughly perpendicular with respect to the membrane initially (Figure 2.2 II, V). Other starting orientations also lead to either a fully wrapped or a half wrapped dumbbell, but the probability for reaching either state was influenced by the initial position as we will discuss below.

If the dumbbell is oriented parallel to the membrane initially ($\theta \approx 90°$) and proceeds to a fully wrapped state, then it tilts in the first part of the engulfment

process to about 60°. Subsequently, its CoM moves inward to almost $d \approx 1.5d_s$ from the undisturbed membrane contour, before returning to a more parallel orientation and an insertion depth about $d \approx 0.7d_s$. This overshooting and recoil is similar to that observed for spheres previously [35,58]. If the dumbbell initially is roughly perpendicular the membrane, it first becomes oriented more precisely perpendicular until it is covered halfway ($d = 0$ and $\theta \approx 10°$) before being wrapped further and finally ending in a more parallel orientation at a similar distance from the undisturbed membrane as the initially parallel dumbbells. Due to the spherical symmetry of the lobes, the point where the membrane peels off from the particle and makes a catenoid-shaped neck with the vesicle is not uniquely determined. Thus, the angle the dumbbell makes with the membrane after having been fully wrapped can vary as it is determined by random processes such as the inhomogeneity of the Neutravidin coating and thermal fluctuations.

For final states where one lobe is being wrapped only, an initially perpendicular dumbbell first reorients more parallel before becoming engulfed until its waist while becoming perpendicular again. An initially parallel dumbbell proceeds to reorient perpendicular while being engulfed, see Figure 2.2b. The gap in the yellow-red trace at $\theta \approx 55°$ and d=0.5 μm was caused by the dumbbell going through an orientation that was filtered out for accuracy as described above.

To obtain more quantitative results for the dynamics of the system we carried out coarse-grained (CG) molecular dynamics (MD) simulations of anisotropic dumbbell particles being wrapped by a membrane. Besides the advantage of easily measuring dynamic properties, in these simulations we are also able to control the size of the vesicle and dumbbell, the membrane tension and the interaction strength between dumbbell and membrane and thus probe a wider parameter space than is available to experiments.

The membrane is modelled using a one particle thick fluid surface developed by Yuan et al [45] which reproduces the mechanical properties associated with biological membranes [50]. Using this model, we simulate spherical membrane vesicles and change the membrane tension by the addition of small solute particles on the inside and outside of the vesicle [138]. The solute particles only interact via volume exclusion and produce a pressure force when the inside and outside concentrations are different. The dumbbell colloid is then placed on the membrane in either a vertical or horizontal initial condition and due to the attractive interaction between the membrane beads and the dumbbell, the dumbbell is slowly wrapped and engulfed by the vesicle. Details can be found in Appendix 2.5.3.

The results obtained from simulations show qualitatively similar behavior as in the experiments, see Figure 2.2. Again, both final states, i.e. i) one lobe attached and ii) fully engulfed, could be reached from any initial position, and the pathway they took was influenced by the initial orientation. Interestingly, our simulations suggest that the initial position strongly influences the first part of the wrapping process and to a lesser degree the second half, which is observed to be similar for both extreme initial orientations. The observation that the wrapping pathways from different initial positions can result in the same final position shows that there is an energy minimum for the GUV-dumbbell system independent of the initial position of the dumbbell. In all observed pathways towards the fully wrapped state, the dumbbell particle tilts during the engulfment suggesting that

this requires less bending energy.

A similar reorientation upon wrapping was observed for linear aggregate of particles [139] and elongated ellipsoids [64,127–129]. Ellipsoids have been found to become first adhered by the side, before rotating to the tip upon being wrapped by the membrane [127]. For sphero-cylindrical particles that were initially touching with their tip, a rotation-mediated wrapping was also seen [48, 66], which can rotate the particle from a standing to a lying position at high aspect ratios. The first point of contact has been predicted to be crucial for the ultimate fate of a non-spherical particle [128,129]. In contrast, for the dumbbell particles used here rotation is not driven by a variation of particle curvature, but primarily by thermal fluctuations and possibly inhomogeneities in the ligand coating density, because of the constant curvature of the constituent spheres of the dumbbells. The only region of curvature variation is the dumbbell neck, which we will show to play a crucial role in the wrapping.

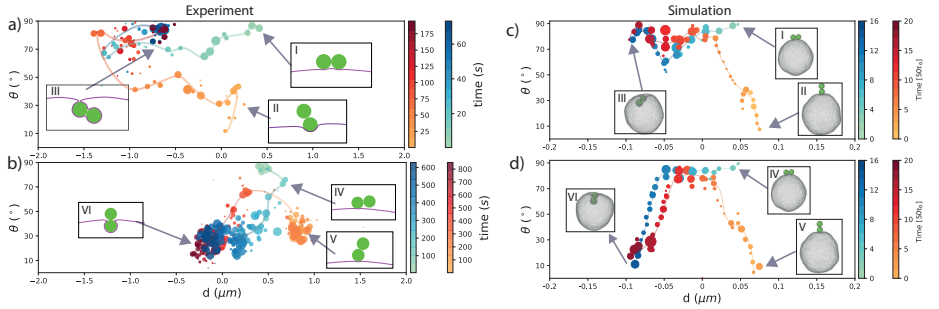

Figure 2.2: Quantitative wrapping pathway of dumbbell particles by GUVs. Tilt angle θ and distance d of the dumbbell from the vesicle surface obtained from a,b) experiments and c,d) simulations as a function of time. In all panels, green-blue pathways indicate dumbbells starting from a vertical position with respect to the vesicle surface, and yellow-red pathways indicate dumbbells that initially start almost horizontally with respect to the membrane. Time is indicated by color and, specified by colorbars for each panel. a) Experimentally obtained pathways for a dumbbell initially oriented parallel (I) or perpendicular(II) to the membrane surface to a fully wrapped end state(III). Each data point represents an average over 1s. b) Experimentally obtained pathways taken by a dumbbell initially oriented parallel (IV) or perpendicular (V) to the membrane surface to the half-wrapped end state (VI). Each data point represents an average over 5s. An alternative presentation can be found in Figure 2.10. c) Simulations of pathways for a dumbbell initially oriented parallel (I) and perpendicular (II) to the membrane surface to the fully-wrapped end state (III). This was the most common stable state with $\sim 90\%$ of dumbbells reaching this end state. d) Simulation of pathways for a dumbbell initially oriented parallel (IV) and perpendicular (V) to the membrane surface to the half-wrapped end state (VI). a-d) Circle size indicates the number of images used for the average and the smooth lines guides to the eye. Simulation time is expressed in τ_0, the MD unit of time.

From the many wrapping processes we observed in experiments and simulations, we identified a number of key intermediate states during the engulfment that ultimately determined the final state. A decisive event during the wrapping of the first lobe is whether the second lobe gets bound to the membrane. This is

always the case if the particle starts out being perfectly parallel and thus with both lobes attached (Figure 2.3A3). If the particle initially is attached with a single lobe (2.3A1 and A2), however, tilting during the engulfment may attach the second lobe (2.3B). In principle, since one lobe is spherical one may expect engulfment to proceed uniformly, not inducing or requiring any tilt. However, any inhomogeneity in the coating density of the ligands on the dumbbells, as well as thermal fluctuations will tilt the particle and may induce contact of the second lobe to the membrane. Since biotin-Neutravidin interactions are essentially irreversible at room temperature, attachment of the second lobe always precludes achieving a final state where only one lobe is wrapped. If the second lobe does not attach, the single-wrapped lobe state is reached (2.3D). Otherwise, the dumbbell will wrap both lobes consecutively, either in a symmetric fashion (2.3E2) or in an asymmetric way (2.3E1), leading to the fully wrapped state. The symmetric wrapping is unstable, and eventually leads to Figure 2.3F in which both lobes are covered. The angle the dumbbell makes with the membrane after wrapping completed can vary. In this end state, a small neck connected the fully wrapped dumbbell at one lobe with the vesicle, see Figure 2.3F.

To quantify the time evolution, we measured the transition times between the different wrapping states. Membrane tension was found to be crucial for the overall wrapping time, see below. Therefore, simulations were used for quantitative measurements of the transition times and experiments for qualitative comparison. While the initial wrapping of the first lobe in the simulations is fast for the different initial states (see Figure 2.3G and H), the wrapping slowed down significantly when the membrane was crossing the waist (Figure 2.3G, B→E1 and H, C→E1). This signifies an energy barrier stemming from the high bending energy required to adapt to the strong variation in curvature of the particle surface. The slowing down at the waist was more significant for the initial condition of a single lobe attached (Figure 2.3G, B→E1) than the initial condition of both lobes attached (Figure 2.3H, C→E1). We observed the same qualitative behavior in experiments, both for tense and floppy GUVs, indicating that the bending energy required to continue wrapping largely exceeded the energy gained from adhesion. In experiments, dumbbells typically wrap within 10 s to 200 s after attachment, depending on membrane tension. Particles wrapped with one lobe (as shown in Figure 2.3D) suddenly transition to the fully engulfed state in less than 10% of these cases within about 10 minutes. In simulation the full engulfment took on average $(790 \pm 30)\tau_0$ and the one-lobe state was stable after $(980 \pm 20)\tau_0$ before the membrane broke due to the large binding energy causing the membrane layer to stretch and tear. Therefore we never observed the transition between states where one lobe is wrapped and where both are fully engulfed within simulations. These observations are in line with ref. [121]. Indeed, we predict that large membrane fluctuations (of the order 100 nm) would be required to transition from the one lobe to the fully wrapped state if the wrapping was to occur completely symmetrically (details of the full calculation can be found in Appendix 2.5.4). The high bending energy costs at the waist and the significantly faster wrapping for tilted dumbbells observed in both simulations and experiments suggest that wrapping a tilted dumbbell is less energetically costly than one that is oriented perpendicular to the membrane. [127] The strong trapping at the waist also causes single-lobe

wrapped dumbbells to attain their stable insertion depth d without overshooting and recoil.

The probability of following a specific pathway and reaching one of the two final states as qualitatively observed in experiments, depended on two factors: the membrane tension of the GUV and the dumbbell's angle θ_0 with respect to the membrane's surface normal during the initial wrapping. The higher the surface tension of the GUV, the more likely it was for the dumbbell to end up in situation 2.3D. Large fluctuations of the vesicle's surface enabled the dumbbell to attach to the non-wrapped lobe. The larger the angle θ in situation 2.3A2, and thus the closer to the membrane it started out at the more likely it was for the dumbbell to end up in situation 2.3B and hence E1.

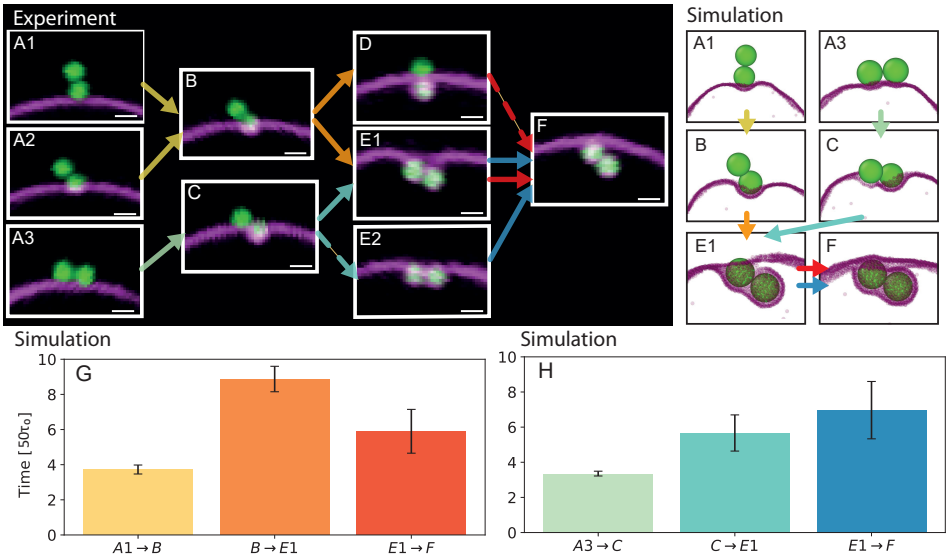

Figure 2.3: Overview of the observed wrapping pathways. A1-F) Confocal images of the possible orientation of a dumbbell (All scale bars denote 1μm). Arrows indicate the directions of the possible wrapping pathways, and dashed arrows illustrate transitions that were rarely observed. G) Measurements of the time between the states for the vertical dumbbell starting position, given in simulation timesteps. H) Measurements of the time between the states for the horizontal dumbbell starting position.

The overall time as well as the transition between different stages in the wrapping strongly depended on the membrane tension - both the initial tension as well as the tension at later times which will increase because of the wrapping, see Figure 2.4. We experimentally measured the membrane tension from the fluctuation spectrum of the lipid vesicle following ref. [28] and plot the time taken to complete wrapping as a function of membrane tension in Figure 2.4a,b. We observed an increase in overall wrapping time with increasing initial membrane tension in experiments (e.g. Figure 2.4a,b) and simulations (Figure 2.4c). However, the range of tensions we could replicate in experiments and simulations was quite limited. To be able to fully explore this effect, we extended a previously developed analytical theory describing the time to wrap colloids [60, 140], which was recently experi-

mentally confirmed [58], and adapted it to the shape of a dumbbell (Details of the theory can be found in the Appendix 2.5.4). In doing so we could explore the effect of tension on time to wrap the dumbbell for a range of theoretical parameters. All the parameters used in the theory were taken directly from the experiment, apart from the binding energy per area (W) and the microviscosity of the membrane (η_{eff}) which are both discussed below.

For a given adhesion energy, we find that the time taken to fully wrap the dumbbell increases non-linearly with the tension. With increasing adhesion energy, the wrapping process becomes faster at the same tension, see Figure 2.4a. The adhesion energies in experiments vary due to the distribution of binding sites between dumbbells [55, 59] which is also reflected in that the experimental data points fall within a range of adhesion energies identified by the theory. We note that only a small percentage of the NeutrAvidin sites that have been added during synthesis contribute to the effective adhesion energy, as was found previously in ref. [55]. Although fixed in the experiments, varying membrane microviscosity in the theory also changes the time taken to wrap. Membrane microviscosity is a measure of how easily the lipids slide past each other during rearrangement, and a higher microviscosity is linked to a higher frictional force during colloid-membrane wrapping. The comparison between the theoretical and experimental results allows us to estimate the membrane microviscosity, which is experimentally inaccessible. We find that our experimental measurements best fit the theoretical curves for a membrane microviscosity of $\eta_{\text{eff}} \approx 0.8$ Pa·s, Figure 2.4b, about 10 times larger than the lower bound estimated in [58]. However, the theory in ref [58] consistently over-estimated the wrapping speed as compared with experiments on spheres, so it could be that the experiment microviscosity was larger than their theoretically predicted value.

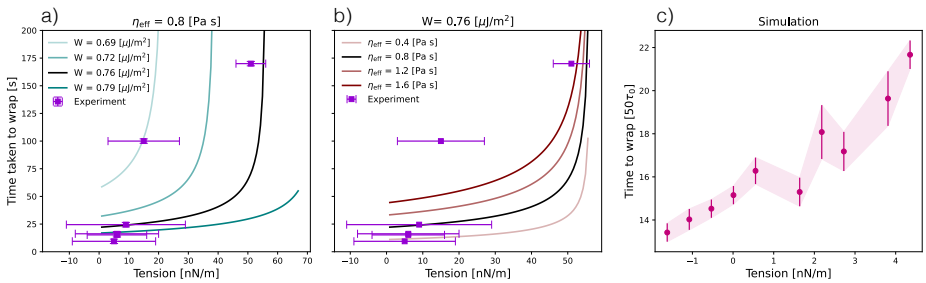

Figure 2.4: Measurement of the time required to fully wrap a dumbbell-shaped particle as a function of membrane tension (a) Experimental data (points) and theoretical predictions (lines) for different adhesion energy per unit area in the range of 0.69-0.79 μJ/m^2 at a fixed membrane viscosity of 0.8 Pa·s. (b) Experimental data (points) and theoretical predictions (lines) for different membrane viscosity in the range of 0.4-1.6 Pa·s at a fixed adhesion energy per unit of area of 0.76 μJ/m^2. (c) Time to fully wrap the dumbbell-shaped particle in simulations for a range of tensions <10 nN/m.

2.4 Conclusion

Here we have developed the first model system to quantitatively study ligand-receptor mediated endocytosis of an anisotropic object by making use of GUVs and colloidal dumbbell particles. We followed and quantified their orientation θ and distance d with respect to the membrane during wrapping using experiments and molecular dynamics simulations. We found that there are two final states: 1) only one lobe or 2) both lobes of the dumbbell are fully wrapped by the membrane. The two states can be reached from any initial position except when both lobes were attached initially which necessarily leads to full wrapping of both lobes. However, the initial position influenced the pathway towards the final state. We identified a number of key intermediate states during the wrapping that determine the final state. Wrapping of one lobe was only found for high membrane tensions and if the other lobe did not touch the membrane during engulfment. Using molecular dynamics simulations we quantified the time required between key intermediate steps, with the slowest step being the crossing of the highly curved neck region of the dumbbell. With simulations we confirmed the experimentally-observed trend of time to wrap increasing for increasing tension, and using analytical theory we estimated the membrane microviscosity.

Our results contribute to a better understanding of how shape affects endocytosis, nutrition uptake, and bacterial evasion. Our choice of a simple anisotropic object, a dumbbell, enabled a key insight: highly negatively curved regions may dominate the wrapping and possibly even prevent full engulfment unless active processes are present. This suggests that objects, such as certain viruses such as pox virus [115]that rely on endocytosis, may profit from having a convex shape. Incorporation of active processes, such as those driven by actin or ESCRT-III polymers, could provide further insights into how the competition between the passive and active processes affects wrapping. In addition, realizing reversible adhesion through a weaker interaction between the membrane and colloids, for example by depletion interactions [57] or weaker, multivalent ligand-receptor based bonds [141], would complement our current understanding of the wrapping of anisotropic particles.

Acknowledgments

This chapter is based on the following publication:
Wrapping pathways of anisotropic dumbbell particles by giant unilamellar vesicles
A. Azadbakht*, B. Meadowcroft*, T. Varkevisser*, A. Šarić, D.J. Kraft
Nano Letters, 3(10):4267-4273(2023). doi:10.1021/ACS.NANOLETT.

I am sincerely grateful to Billie Meadowcroft and Anđela Šarić for their invaluable contributions in performing simulations and the theoretical model for wrapping dummbells, and for the insightful discussions and writhing the article. I also thank Thijs Varkevisser for his extensive work on experimental data acquisition and analysis as part of his master's project. I thank Casper van der Wel for providing

*These authors contributed equally.

open-source packages for tracking, as well as Yogesh Shelke for his assistance in preparing PAA coverslips and Rachel Doherty for her assistance with particle functionalization.

2.5 Appendices

2.5.1 Quantification of specific binding affinity

The NeutrAvidin functionality was confirmed using the specific binding affinity to biotin, by showing that the particles were wrapped by biotin-functionalised GUVs. The average amount of binding sites per particle was quantified by titration analysis, using the same method discussed in [59].

First, NeutrAvidin-functionalised particles were dispersed with a concentration of 0.05% w/w in PBS and different amounts of biotin-4-fluorescein were added to the particles. The mixture was then incubated for 20 minutes at 55 °C. After incubating, the particles were sedimented by centrifuging and the supernatant was collected. The fluorescence of the diluted supernatant was subsequently measured using fluorescence spectrophotometry. The added amounts of biotin-4-fluorescein were selected such that some amounts were completely absorbed by the NeutrAvidin-functionalised particles, while others remained partly in the supernatant. A horizontal baseline and a linear function were fitted, respectively, to the two sections. The amount of absorbed biotin, and thus the binding affinity of the particles was determined from the intersection point of both fits. The absorbed biotin was 23.5 pmol mg^{-1} which implied an average amount of 7.3×10^3 binding sites per spherical particle, and twice that amount for dumbbells. Assuming 17 k_BT per avidin-biotin bond [142], the adhesion energy per unit area was estimated to average 156 $\mu J/m^2$, which is well above the critical value for wrapping one sphere. It is worth mentioning in earlier work on the same system [55], it was found that there is an order of magnitude spread in the Neutravidin coating density of particles. Moreover, after applying the Neutravidin coating, we subsequently stabilize the particles against aggregation with an additional layer of PEG polymers discussed in Particle Functionalization. These polymers are likely to partially block access and thus adhesion of biotinylated lipids to the Neutravidin. The titration assay of the Neutravidin density with fluorophores functionalized with biotin are more likely to still bind due to their much smaller size and greater freedom to move compared to the biotinylated lipids in the membrane, which leads to an overestimation of the accessible Neutravidin on the particle surface. This overestimation may further be enhanced by the fact that at least three out of the four Neutravidin binding pockets will be oriented such that access to them is obstructed by the polymer coating. The earlier study showed that only 2% of the linkers are able to effectively adhere to the ligands in such an experimental system [55].

The results of the fluorescence measurements and the two fits are illustrated in Figure 2.5. The baseline has a non-zero value as the biotin-4-fluorescein had the same emission wavelength as the fluorescent dye included in the particles, and some of the particles remained within the supernatant after centrifuging.

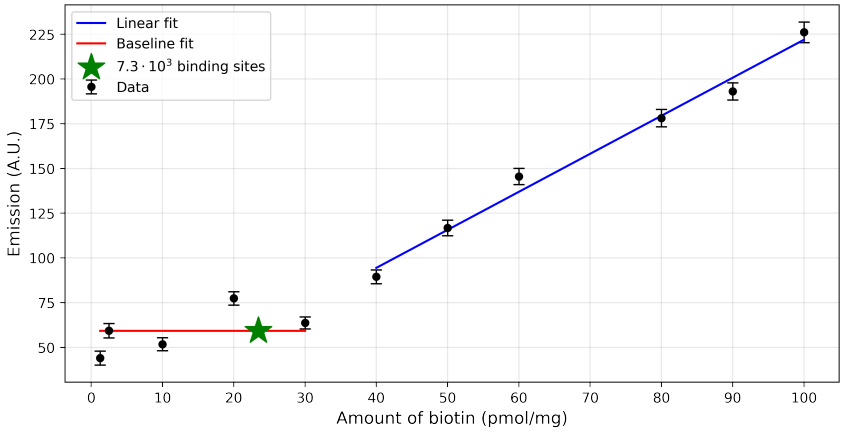

Figure 2.5: Emission intensity of the supernatant of biotin-4-fluorescein (b4f) incubated, NeutrAvidin-functionalised particles for different amounts of b4f. The baseline is fitted for the amounts of b4f that were completely adsorbed to the particles. The linear function is fitted to amounts where some b4f remained in the supernatant after centrifugation. The green star indicates the intersection of the two fits, and corresponds to 7.3×10^3 binding sites per spherical particle.

2.5.2 Quantification of dumbbell wrapping

We quantified the wrapping process by measuring the dumbbell's angle θ with respect to the membrane's surface normal and the distance d between the dumbbells center of mass (CoM) and the membrane. To do so, we first measured the GUV radius R and its center by fitting a 3D confocal Z-stack with a sphere using the Python package circletracking [136]. Subsequently, we tracked the position of the two lobes of the dumbbell using the Python package clustertracking [135] for each time frame and from this calculated the position of the dumbbell's center of mass (CoM) in time. Measuring the cross-section radius r of the GUV in each frame, see Figure 2.1f, we determined the distance of the dumbbell from the equator of the vesicle in z, through $z = \sqrt{R^2 - r^2}$, since measuring of z allowed a 3D tracking of all parameters. In addition, because the quality of the contours decreases far from the equator, the particles were tracked only when $-0.8R<z<0.8R$. Then, given R and a dumbbell CoM distance to the centre of this sphere q, the dumbbell CoM distance d to the vesicle can be defined as

$$\mathrm{d} = q - R \tag{2.1}$$

Knowing the absolute position of the dumbbell and vesicle in three dimensions, we can calculate the distance of the dumbbell's CoM from the undistorted membrane contour, d, as well as the angle θ between the major axis of the dumbbell and surface normal of the GUV, which are depicted in Figure 2.1d. We approximated the position of the membrane in the vicinity of the dumbbell-induced deformation by fitting a circle to the membrane. We note that we only analyzed frames where the dumbbell was approximately in the confocal plane. Since the fluorescence in-

tensity decreases as an object moves out of focus, we selected frames for analysis where the intensity of both spheres were not lower than 75% of the maximum intensity of each lobe and differed by no more than 20% from their average intensity. In this way, the precision of θ was increased, with a maximum error of 19°. For details, see below Experimental image filtering.

Due to the indentation of the membrane induced by the dumbbell, the membrane's contour deviated from a perfect circle. Therefore, we locally fitted the membrane contour in the vicinity of the particle to obtain a more accurate results of d. To do so, we disregarded the highly deformed membrane contour in the direct vicinity of the particle up to 3.5μm around the CoM, see Figure 2.6. The negative bias induced by the global circle fit was prevented by ignoring this contour. Additionally, a contour of azimuthal angle more than $\pm 36°$ away from the particle was also disregarded in the local circle fit, such that the circle approximated the contour in the vicinity of the dumbbell as well as possible, indicated with yellow dots in Figure 2.6.

Figure 2.6 shows both the globally and the locally fitted circle for a tense and a floppy vesicle. The yellow dots illustrate the selected contour to which the local circle fit was performed. The Figure also shows that in the case of a tense vesicle without any wrapped particles (the depicted dumbbell is attached only), the global and local circle fits well. However, the locally fitted circle approximated the contour around the particle better than the global circle fit for the floppy vesicle with a partly wrapped dumbbell. For this reason, the locally fitted circle was used to calculate the dumbbell's center of mass distance d to the GUV's surface.

Experimental image filtering

GUV radius filtering To prevent substantial errors in the GUV contour determination due to noise, only frames around the equator were used. The selection of suitable frames was made by fitting the vesicle contour for all frames with a circle and comparing it to the radius R of the GUV obtained from fitting a sphere to a z-stack. Images where the radius of the circle was smaller than $0.8R$ were not used in the analysis. The boundary value of 80% was determined by manually assessing the quality of multiple GUV contours at various distances from the equator. A further increase in selectivity to images whose radius falls within 90% of the vesicle radius is shown in Figure 2.7b but did not further improve reduction of noise. Thus, we selected images where the radius of the vesicle fell within $0.8R$ for the whole chapter.

Filtering related to dumbbell intensity To ensure high precision of the quantitative analysis of the dumbbell wrapping process, we proceeded as follows: we used the particle tracking algorithm to determine the coordinates as well as to calculate the intensities of both lobes. The coordinates were determined by fitting a Gaussian to the intensity profiles, and the sum of all the pixel intensities within a profile was reported as the lobe intensity. We then applied two filtering steps to ensure that the dumbbell lobes were at the same height and located in the focal plane.

To improve the accuracy of the z-position, we selected frames where both

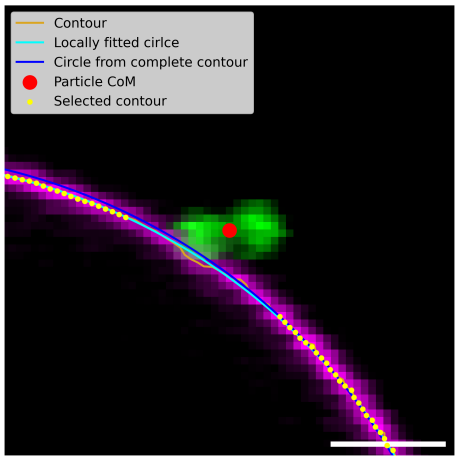

(a) Tense vesicle, close-up of (B)

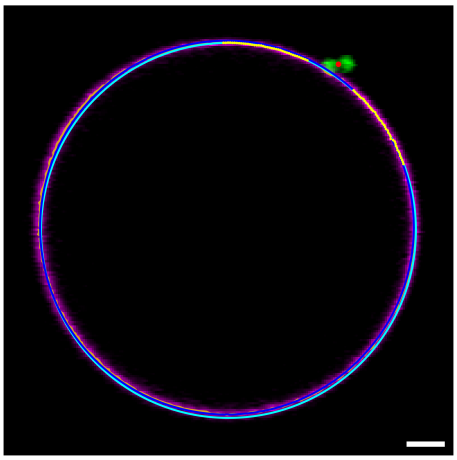

(b) Tense vesicle

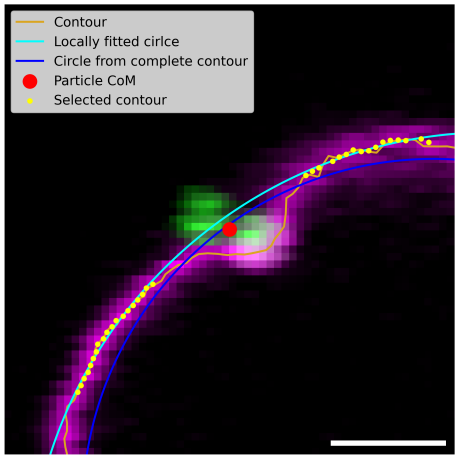

(c) Floppy vesicle, close-up of (D)

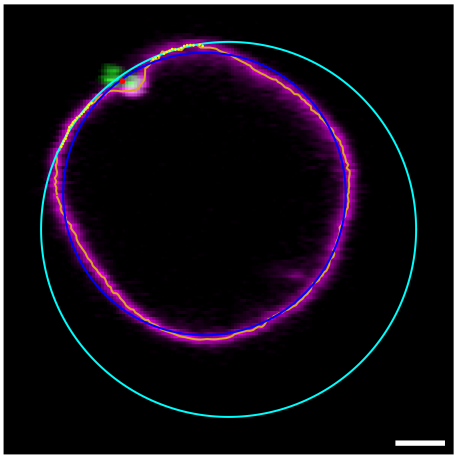

(d) Floppy vesicle

Figure 2.6: Confocal images illustrating the global and local circle fit for a (A,B) tense vesicle and a (C,D) floppy vesicle. The dumbbell particles are depicted in green and the vesicle in magenta. For the tense GUV without any wrapped particles, the locally fitted circle and the circle fitted to the complete contour both match the contour around the particle very well. For the floppy vesicle with the (partly) wrapped particle, the locally fitted circle matched the contour around the particle better than the global circle fit. The contour used to locally fit the circle is highlighted with yellow dots. All scale bars denote 2 µm.

dumbbell lobes were at the same height and within error in the optical focal plane of the objective lens. This was accomplished by selecting frames where the intensity of the spheres was within 75% of the maximum lobe intensity observed in a z-stack scan of the GUV-dumbbell system. A further increase in the filter value to 85% of the maximum lobe intensity does not further reduce the noise but only removes additional data points, see Figure 2.7 c.

To make sure that the two lobes of the dumbbells were both located in the focal plane, we introduced a relative intensity filter. To do so, we measured the mean normalized intensity of the two spheres in every frame and removed those frames where a normalized lobe intensity deviated more than 20% from the mean intensity. Reducing the cutoff value to 10% of the mean normalized intensity does not lower the noise in θ as shown in Figure 2.7 d. Therefore, we chose a value of 20%.

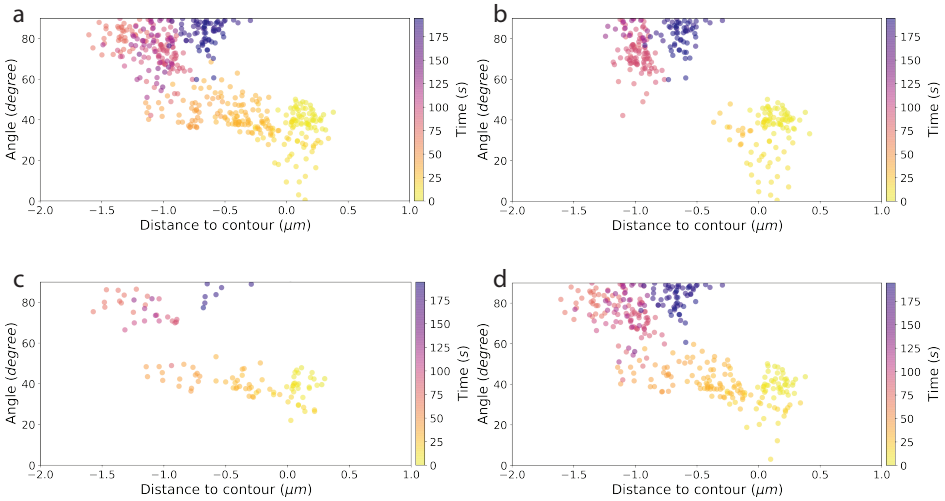

Figure 2.7: Quantitative wrapping pathways as presented in Figure 2.2a for different filter settings. Depicted are θ and d as a function of time, which is indicated by color coding. . (**a**): The pathways for the default filter values in which the radius of the circle was not allowed to be smaller than 80% of the actual GUV radius, the sphere intensity had to be higher than 75% of the maximum intensity of each lobe, and the relative dumbbell lobe intensity had to be higher than 80% of the mean intensity value. (**b-d**): Pathways for different settings of the filter values. (**b**) Frames with GUV crossesctions smaller than $0.9R$ were filtered out. (**c**) Frames where lobes with an intensity that was below 85% of the maximum lobe intensity were filtered out. (**d**) Frames where the relative intensity deviation of each lobe was less than 90% of the mean normalized intensity were filtered out. None of the increased filter boundary values resulted in a significantly reduced fluctuations of the angle-distance data.

Analysis of measurement error in θ We estimated the error in θ by measuring the error in the relative height of the two dumbbell lobes. To do so, we first measured the average lobe intensity as a function of z by scanning a single sphere in steps of 1 nm with confocal microscopy. 12 separate z-stack image sequences

were used to determine the average intensity as a function of the z height relative to the sphere's maximum intensity value, see Figure 2.8a. This maximum value was determined by fitting a parabola to the intensity. We set the z coordinate corresponding to the maximum of the parabola as the value the sphere would have if it is in the focal plane during a measurement of the wrapping process, i.e. $z = 0$. The standard deviation from these 12 measurements relative to the average intensity is depicted in Figure 2.8b.

The standard deviation (stdev) in the average intensity implies that the z-position of the two lobes of the dumbbells can only be determined up to that value through this method. For $z = 0$, the value of the normalised standard deviation stdev$(z = 0) = 0.05$ corresponds to an error in the z-coordinate of ± 159 nm. Such a deviation in the z-position corresponds to a maximum measurement uncertainty in the angle $\Delta\theta = 19°$ between the dumbbell long axis and the focal plane when the dumbbell lies approximately in the plane, see Figure 2.9.

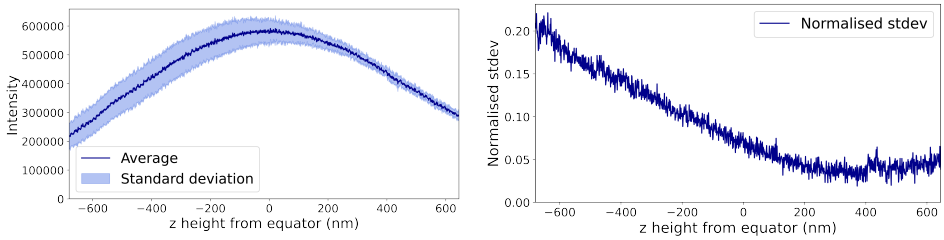

(a) Single particle intensity

(b) Average-normalised standard deviation

Figure 2.8: The average intensity and standard deviation from 12 z-stack image sequences of a single fluorescent spherical particle. (**a**): The average intensity and standard deviation as a function of the z height from the particle equator. $z = 0$ was determined by fitting a parabola to the average intensity and using the maximum value. (**b**): The standard deviation normalized by the average intensity as a function of the z height.

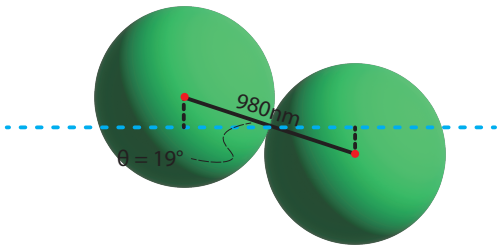

Figure 2.9: Illustration of error in the angle θ of a dumbbell with the focal plane (dashed blue line) given a standard deviation of 159 nm for the z-coordinate.

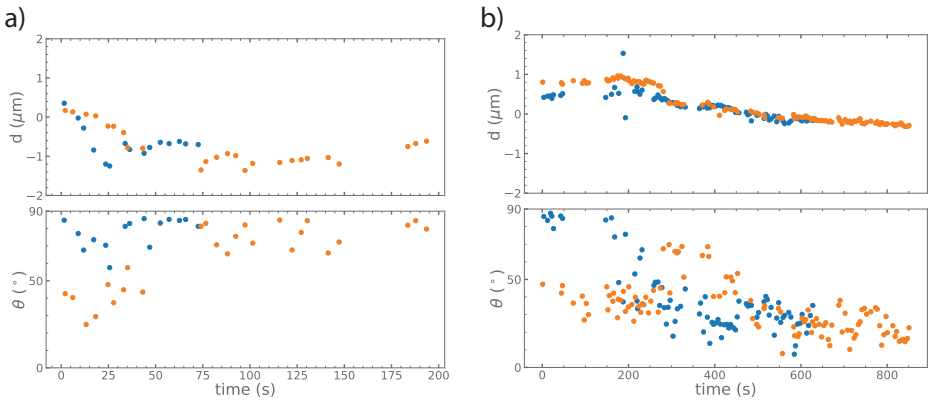

Figure 2.10: Alternative presentation of the data shown in Figure 2.2 a) and b) of the main text. Distance d of the dumbbell from the vesicle surface and tilt angle θ as a function of time obtained from experiments. The orange data points are initially perpendicular to the vesicle, and the blue data points are oriented parallel to the membrane. a) Experimentally obtained pathways for a dumbbell initially oriented parallel (blue) or perpendicular (orange) to the membrane surface to a fully wrapped end state. Each data point represents an average over 1s. b) Experimentally obtained pathways taken by a dumbbell initially oriented parallel (blue) or perpendicular (orange) to the membrane surface to the half-wrapped end state. Each data point represents an average over 5s.

2.5.3 Simulations details

We ran molecular dynamics simulations using LAMMPS [143] and explored a membrane vesicle wrapping a dumbbell-shaped colloid. The membrane was modelled using a 1-bead thick membrane model developed by Yuan et al [45] which models an implicit solvent with a single anisotropic pair interaction potential. The parameters for the membrane were as follows: $\sigma = 1$, $r_{\text{cut}} = 2.6$, $r_{\text{min}} = 1.12$, $\mu = 3$, $\zeta = 4$, $\epsilon = 4.43$, following the notation in the original paper. The membrane vesicle is made of $N = 9722$ beads. The dumbbell was a single rigid body consisting of two spheres, each with a diameter $\sigma_{\text{dumbb}} = 7.5\sigma$. We convert this to real units in Figure2.2 using $\sigma = 10$ nm. The mass of each dumbbell sphere was 30× larger than one membrane bead. The dumbbell interacted with the membrane at a distance r_{ij} via a cut-and-shifted Lennard-Jones potential: $E_{ij} = 4\epsilon((\frac{\sigma}{r_{ij}})^{12} - (\frac{\sigma}{r_{ij}})^{6}) - E_c$, $r_{ij} < r_c$ where $E_c = 4\epsilon((\frac{\sigma}{r_c})^{12} - (\frac{\sigma}{r_c})^{6})$. The cutoff was chosen to be $0.65(\sigma + \sigma_{dumbb})$. To qualitatively match the experimental wrapping pathways we found the optimal interaction strength to be $\epsilon = 8k_{\text{B}}T$. The simulations typically ran for $200000\Delta\tau$ where $\Delta\tau = 0.01\tau_0$ (τ_0 is the MD unit of time). The simulations were performed in the canonical ensemble with periodic boundary conditions by coupling an NVE setup and a Langevin thermostat using a friction coefficient $\gamma = \frac{m}{\tau_0} = 1$. The simulation box is a cube with a fixed edge length of $L_{\text{box}} = 92\sigma$.

For the quantification of the time taken between states during the wrapping pathway (Figure 2.3), we defined the states when the dumbbell reached particular

thresholds of d and θ, the values of which we outline here. For the pathway of dumbbells starting in the vertical position, the initial state change is that from vertical (state A1, $\theta = 0°$) to tilted (state B, $\theta = 40°$). The dumbbell then gets more tilted and sinks into the membrane (state E1, $\theta = 65°$, $d = -6\sigma$) before sinking to its final position (state F, $d = -8.5\sigma$). For the pathway of dumbbells starting in the horizontal position the first state change is that of the dumbbell sinking from sitting above the vesicle contour (state A3, $d = 5\sigma$) to be in line with the vesicle contour (state C, $d = 0°$). The dumbbell then sinks more and tilts (state E1, $\theta = 65°$, $d = -6\sigma$) before reaching its final position (state F, $d = -8.5\sigma$).

In Figure 2.4 c) we measure the time to wrap the dumbbell for different membrane tensions. The different tensions are realised by placing small solute beads with different concentrations in and outside the membrane vesicle. These particles interact only via volume exclusion and thereby behave as a gas and have the sole effect of creating a pressure difference between the in and outside leaflet of the membrane. The pressure difference can be calculated using $\Delta\Pi = \mathrm{RT}(\rho_{\mathrm{in}} - \rho_{\mathrm{out}})$ where $\Delta\Pi$, RT and $\rho_{\mathrm{in/out}}$ are the pressure difference, the ideal gas constant multiplied by temperature and the concentration of particles in/out, respectively. We then use Laplace's law to relate this pressure difference to tension, namely $\mathrm{Tension} = \frac{\Delta\Pi r_{\mathrm{ves}}}{4}$ where r_{ves} is the radius of the membrane vesicle.

2.5.4 Effect of membrane tension on time taken to fully wrap

Summary of theory for time taken to wrap the dumbbell

Previous works have developed theory to estimate the time it takes membranes to adhere and fully wrap colloids [60]. Recently, a thorough study calculated the time to wrap a spherical particle including comparison to experiments, estimates of experimentally inaccessible parameters and an in-depth discussion about the relevance of the theory in different regimes [58]. Another theoretical work looked at the time to wrap non-spherical objects including cylinders [144] and further addressed stochastic effects within this model [140]. Here, we employ the same theoretical framework as those in the above published works and apply it to a dumbbell-shape colloid. The theory calculates the uptake force, which is a function of the bending energy and stretching energy of the membrane as well the binding energy of the membrane and colloid. This uptake force is then equated to an effective friction force which acts at the contact line between the colloid and the adhering membrane. Experiment has shown that this contact line moves approximately at a linear speed so that the friction force has an effective constant viscosity, η_{eff}. In general, the time taken to wrap depends on the geometry and size of the particle, the adhesion energy per area, W, the bending rigidity of the membrane, κ, the tension of the membrane, σ, and the micro-viscosity of the membrane, η_{eff}. The non-adhered membrane bending is ignored, as it has been shown that it contributes to up to ~ 20 % of the total membrane bending [144].

We take the radius of each sphere of the dumbbell ($R = 0.5\mu$m) and tensions (0-50 nN/m) directly from experimental measurement. We assume the bending

rigidity is similar to most membranes at $20k_BT$. In the experiment, the tension was reduced via osmosis until the membrane was able to wrap and engulf the particles. Therefore we assume that the particle-membrane system is near the critical adhesion energy needed for wrapping. In this system the critical adhesion energy per area for particle engulfment is $w_c \sim \frac{2\kappa}{R^2} + \sigma = (0.65 - 0.7)\mu\text{J/m}^2$ for the experimental tension range. We therefore vary the adhesion energy per area near to and slightly above this value. The final parameter needed to calculate the time to wrap is the membrane microviscosity. This value represents how easily lipids rearrange near the contact line between colloid and membrane. The effective viscosity is difficult to measure experimentally and has been previously estimated for only a handful of membranes [58, 145, 146]. Varying the value of the microviscosity we find that the theory best fits the experimental measurements for values of $\eta_{\text{eff}} \sim$0.8 Pa s which is 10 times larger than that estimated in [58], $\approx$ 0.08 Pa s.

Calculation of time taken to wrap the dumbbell

We based our calculations on a theory previously developed in [60] and extended in [140]. Below is a summary of the ingredients and assumptions of this analytical theory and an outline of how we extended the theory for use with a dumbbell shape.

The main assumption in the theory is that there is a thermodynamic driving force, calculated from the derivative of the total energy of the system with respect to an appropriate line element, and that this can be equated to a frictional force. The frictional force can be calculated when the contact line between the colloid and membrane is moving at constant speed. In this case there is a microviscosity that linearly relates the speed of the contact line with the force exerted on it.

We assume that the membrane in the vicinity of the dumbbell is locally flat with an intrinsic mean curvature of zero. The total energy of the system can be written as follows:

$$E_{\text{tot}} = -\int_{A_d} W \mathrm{d}A + \int_{A_d} 2\kappa H^2 \mathrm{d}A + \sigma \Delta A \tag{2.2}$$

Where the first term is the colloid-membrane adhesion energy, W is the adhesion energy per area and A_d is the colloid-membrane attached area. The second term is the membrane bending where κ is the membrane bending rigidity and H is the membrane mean curvature. The third term is the membrane stretching term where σ is the membrane tension and ΔA is the change in area from the flat membrane state.

For a given choice of parametrisation, which is dependent on the specific geometry of the system, we define the contact line between colloid and membrane (the line of the front of membrane attachment), with length l_{cl}, as moving in the direction of the line segment s. The frictional force can therefore be written as:

$$F_{\text{fric}} = \eta_{\text{eff}} l_{\text{cl}} \dot{s} \tag{2.3}$$

And we relate the total energy and frictional force via:

$$F_{\text{fric}} = -\frac{\mathrm{d}E_{\text{tot}}}{\mathrm{d}s} \tag{2.4}$$

To solve these equations for the shape of a dumbbell, we separate the shape into two spheres with a small cylindrical neck in between, as shown in Figure 2.11b. We then parameterise the above equations using θ, as shown in 2.11a, for the spherical shapes and z, the z-axis of the cylinder, for the cylindrical neck. We assume the membrane wraps these shapes consecutively, and therefore we can solve the equation for each shape with the appropriate initial and final positions of the contact line, and add the resulting times. For example, the equation for the cylinder will read:

$$\begin{aligned}\eta_{\text{eff}} l_{\text{cl}} \dot{z} &= -\frac{\mathrm{d}E_{\text{tot}}}{\mathrm{d}z} \\ &= 2\pi R_{\text{cyl}}(W - \sigma - \frac{\kappa}{2R_{\text{cyl}}^2})\end{aligned} \tag{2.5}$$

The contact line in this case is $l_{\text{cl}} = 2\pi R_{\text{cyl}}$, so that this equation simplifies to $\dot{z} = \frac{w-\sigma}{\eta_{\text{eff}}} - \frac{\kappa}{2\eta_{\text{eff}} R_{\text{cyl}^2}}$ and the time is calculated from $T = \int_0^{h_{\text{cyl}}} (1/\dot{z})\mathrm{d}z$. We can write the total time to wrap as follows:

$$\begin{aligned}T_{\text{wrap}} = &\int_0^{\frac{\pi}{2}+\arccos\left(\frac{R_{\text{cyl}}}{R_{\text{sph}}}\right)} \frac{1}{\nu_{\text{up}} - \nu_\sigma(1-\cos\theta)}\mathrm{d}\theta \\ &+ \int_0^{h_{\text{cyl}}} \frac{1}{\nu_{\text{up}}^{\text{cyl}}}\mathrm{d}z \\ &+ \int_{\frac{\pi}{2}-\arccos\left(\frac{R_{\text{cyl}}}{R_{\text{sph}}}\right)}^{\pi} \frac{1}{\nu_{\text{up}} - \nu_\sigma(1-\cos\theta)}\mathrm{d}\theta\end{aligned} \tag{2.6}$$

Where, as defined in [140], $\nu_{\text{up}} = \frac{w}{R_{\text{sph}}\eta_{\text{eff}}} - \frac{2\kappa}{R_{\text{sph}}^3\eta_{\text{eff}}}$, $\nu_\sigma = \frac{\sigma}{R_{\text{sph}}\eta_{\text{eff}}}$ and $\nu_{\text{up}}^{\text{cyl}} = \frac{w-\sigma}{\eta_{\text{eff}}} - \frac{\kappa}{2\eta_{\text{eff}} R_{\text{cyl}^2}}$.

This can be solved analytically which gives rise to the plots in Figure 2.4. A list of the parameters used for the theory can be found in table S1. The solutions reflect that near to the critical adhesion energy the time to wrap diverges and therefore small changes in W or σ will give rise to large changes in the time to wrap. This can be seen in 2.12 which shows the time to wrap near the critical regime for different tensions, and far from the critical regime.

2.5.5 Estimating the energy barrier at the dumbbell neck

Our experiments and MD simulations both show a 1-lobe wrapped state that is stable for some time. This suggests that there is an energy barrier to reach the fully wrapped global energy minimum from this local minimum. Here, we use the

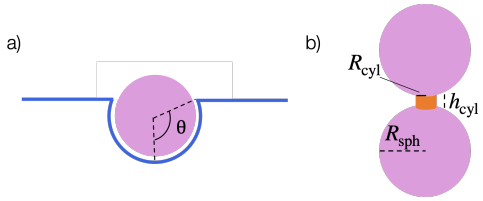

Figure 2.11: Shapes for the theoretical time to wrap calculation. a) For the spherical geometry, we define θ from 0, when the sphere is only just in contact with the flat membrane, to π when the sphere is fully engulfed by the membrane. b) For the dumbbell geometry there are three key geometric parameters: the radius of the sphere (R_{sph}), the radius of the cylinder between the two spheres (R_{cyl}), and the height of this cylinder (h_{cyl}).

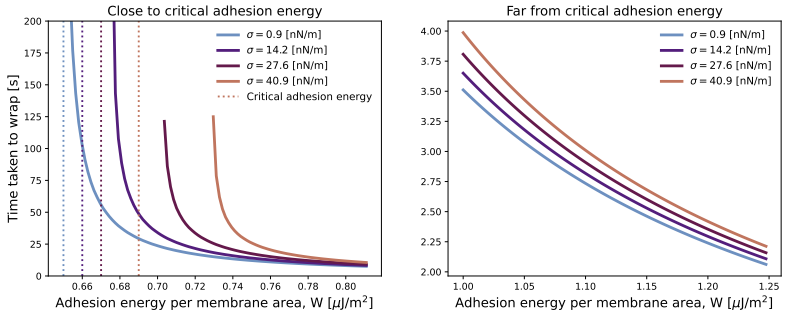

Figure 2.12: Solutions to Equation (6) in two regimes. Time to wrap the dumbbell close to the critical adhesion energy for wrapping (left) and far from the critical adhesion energy (right). The time to wrap diverges at the critical adhesion energy, W_{c}, which is different for different tensions.

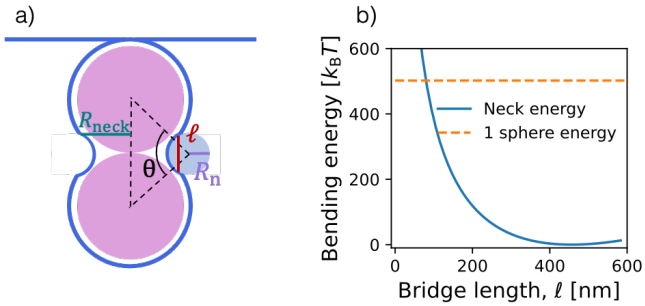

Figure 2.13: Estimating the energy barrier for wrapping the full dumbbell from the 1-lobe wrapped state. The geometry we assume for the energy barrier calculation is shown in a), with the 'bridge length', ℓ, in red. The bending energy barrier is shown in b) for varying bridge lengths. This is compared with the bending energy of one sphere.

Table 2.1: Theory and Simulation parameters

Parameter	Simulation value	Theory value
Membrane rigidity	$17k_{\mathrm{B}}T$	$\kappa = 20k_{\mathrm{B}}T$
R_{sph}	$3.75R_{\mathrm{bead}}^{\mathrm{membrane}}$	$0.5\,\mu$m
R_{cyl}, h_{cyl}		$0.025\,\mu$m, $0.05\,\mu$m
Tension	$18k_{\mathrm{B}}T/(2R_{\mathrm{bead}}^{\mathrm{membrane}})^2$	$\sigma = 10\,$nN/m
Adhesion energy	$8k_{\mathrm{B}}T$/membrane bead	$W \approx 0.7\,\mu\mathrm{J/m}^2$
Membrane Viscosity		$\eta_{\mathrm{eff}} \approx 0.8\,\mathrm{Pa}\cdot\mathrm{s}$

Helfrich model for membrane bending to estimate an upper bound for this barrier. For simplicity we neglect surface tension. We assume that to continue wrapping after the first lobe has already been symmetrically wrapped (the 1-lobe state), the membrane at the surface of the dumbbell must at some point on detach and bridge to the next lobe in order to not take on the high bending cost of wrapping close to the neck region. We constructed an argument in terms of a 'bridge length', ℓ (see Figure 2.13a), which we take as the length at which the wrapped 1-lobe membrane may 'see' the next lobe through fluctuations, and can reach the state of two lobes wrapped.

$$\begin{aligned}\mathcal{H}_{\mathrm{neck}} &= \frac{\kappa}{2}\int_{\mathrm{Neck}} \mathcal{C}^2 \mathrm{d}A \\ &= \frac{\kappa}{2}\left(\frac{1}{R_{\mathrm{n}}} - \frac{1}{R_{\mathrm{neck}}}\right)^2 A\end{aligned} \tag{2.7}$$

We choose to write all functions and variables in terms of θ, R_{n} and R_{sph} where $\theta = \arccos\left(1 - \frac{2R_{\mathrm{sph}}}{(R_{\mathrm{sph}}+R_{\mathrm{n}})^2}\right)$ is the angle the dumbbell spheres make with the sphere that defines the neck region (see Figure 2.13a), R_{n} is the radius of this sphere and R_{sph} is the radius of the dumbbell sphere. The area of the neck region can be written as follows:

$$A = R_{\mathrm{n}}\theta \times 2\pi R_{\mathrm{sph}} \sin\left(\frac{\pi - \theta}{2}\right) \tag{2.8}$$

Finally, we plot $\mathcal{H}_{\mathrm{neck}}$ as a function of the 'bridge length' which can be written, $\ell = 2\pi R_{\mathrm{n}} \sin\frac{\theta}{2}$.

As is shown in Figure 2.13b, the neck energy increases dramatically for a bridge length of less than 200 nm. It reaches a minimum (zero) when the membrane takes on the shape of a catenoid, $R_{\mathrm{neck}} = R_{\mathrm{n}}$. These calculations predict a large energy barrier to reach the two lobe state from the 1-lobe state for membrane fluctuations on the order of less than 100 nm. The energy barrier shown here is a generous upper bound as it assumes the membrane would need to span the whole neck region all at once and in reality the dumbbell probably tilts in a step-wise fashion to wrap the second lobe.